




Charge and spin gaps in the ionic Hubbard model with density-dependent hopping

O. A. Moreno Segura 


Centro Atómico Bariloche and Instituto Balseiro, 8400 Bariloche, Argentina

K. Hallberg 

Instituto de Nanociencia y Nanotecnología CNEA-CONICET, Centro Atómico Bariloche and Instituto Balseiro, 8400 Bariloche, Argentina

A. A. Aligia 

Instituto de Nanociencia y Nanotecnología CNEA-CONICET, GAIDI, Centro Atómico Bariloche and Instituto Balseiro, 8400 Bariloche, Argentina

 (Received 19 September 2023; revised 19 October 2023; accepted 3 November 2023; published 17 November 2023)

We calculate the charge gap ΔE_C and the spin gap ΔE_S of the ionic Hubbard chain including electron-hole symmetric density-dependent hopping. The vanishing of ΔE_C (ΔE_S) signals a quantum critical point in the charge (spin) sector. Between both critical points, the system is a fully gapped spontaneously dimerized insulator. We focus our study in this region. Including alternation in the hopping, it is possible to perform an adiabatic Thouless pump of one charge per cycle, but with a velocity limited by the size of the gaps.

DOI: [10.1103/PhysRevB.108.195135](https://doi.org/10.1103/PhysRevB.108.195135)

I. INTRODUCTION

The ionic Hubbard model (IHM) consists of the usual Hubbard model with on-site Coulomb repulsion U supplemented by an alternating one-particle potential Δ . It has been used to study the neutral-to-ionic transition in organic charge-transfer salts [1,2] and the ferroelectric transition [3]. More recent studies have established that the chain at half filling has three different thermodynamic phases, and different gaps, correlation functions, and other properties have been studied [4–12]. The unit cell consists of two sites with on-site energies $\pm\Delta$. Chains with larger unit cells have also been studied [13,14].

The model studied in this paper is the IHM with density-dependent hopping (DDH). It is the version without alternation of the hopping ($\delta = 0$) of the interacting Rice-Mele model [15] including DDH. Because of its relevance for quantized charge pumping, we describe the full Hamiltonian, also including δ , as

$$\begin{aligned}
 H = & \sum_{j\sigma} [-1 + \delta (-1)^j] (c_{j\sigma}^\dagger c_{j+1\sigma} + \text{H.c.}) \\
 & \times [t_{AA}(1 - n_{j\bar{\sigma}})(1 - n_{j+1\bar{\sigma}}) + t_{BB}n_{j\bar{\sigma}}n_{j+1\bar{\sigma}} \\
 & + t_{AB}(n_{j\bar{\sigma}} + n_{j+1\bar{\sigma}} - 2n_{j\bar{\sigma}}n_{j+1\bar{\sigma}})] \\
 & + \Delta \sum_{j\sigma} (-1)^j n_{j\sigma} + U \sum_j n_{j\uparrow}n_{j\downarrow}. \quad (1)
 \end{aligned}$$

The first term is the DDH, which is alternating for $\delta \neq 0$. The amplitudes t_{AA} , t_{AB} , and t_{BB} correspond to hopping of a particle with a given spin, when the total occupancy of both sites for particles with the opposite spin is 0, 1, and 2, respectively. In the following, we assume the electron-hole symmetric case $t_{BB} = t_{AA}$, which is the one implemented experimentally with cold atoms [16–20]. Δ is the alternating on-site energy and U

is the on-site Coulomb repulsion. $t_{AB} = 1$ will be taken as the unit of energy.

The model with $\Delta = \delta = 0$ has been derived and studied in two dimensions as an effective model for cuprate superconductors [21–24]. In one dimension, also, superconductivity is favored for some parameters [25–29]. Our interest in DDH here is that for t_{AB} larger than the other two, the fully gapped spontaneously dimerized insulating (SDI) phase is favored [30–34]. This is important for fully adiabatic quantized charge pumping of one charge. So far, charge pumping has been studied in the interacting Rice-Mele model in the absence of DDH ($t_{AA} = t_{AB} = t_{BB}$) [35–38].

The well-studied IHM [Eq. (1) with $\delta = 0$ and $t_{BB} = t_{AA} = t_{AB}$] has three phases: the band insulating (BI) phase, the Mott insulating (MI) phase, and a narrow spontaneously dimerized insulating (SDI) phase in between. An intuitive understanding of the first two phases is provided by the zero-hopping limit, in which the occupancies of the different sites are 2020... (BI phase) for $\Delta > U/2$ and 1111... (MI phase) for $\Delta < U/2$. For finite hopping, the SDI phase appears in between, as first shown by bosonization [4] and described in more detail later using an approximate mapping to an SU(3) Heisenberg model [8,9].

The phase diagram of the model has been constructed in Ref. [5] using the method of crossings of excited energy levels (MCEL) based on conformal-field theory [30,39–42]. For this model (also including density-dependent hopping), the method also coincides with that of jumps of charge and spin Berry phases used in Ref. [31]. The basis of the MCEL is that in one dimension, the dominant correlations at large distances correspond to the smallest excitation energies. Thus, the crossings of excited levels in appropriate symmetry sectors therefore correspond to phase transitions. The Lanczos algorithm, using total wave vector, inversion symmetry [43], and

time-reversal symmetry, has been used in order to separate the different symmetry sectors, limiting the maximum size to 16 sites. The results were obtained extrapolating to the thermodynamic limit [5]. Open-shell boundary conditions (OSBCs) were used, which correspond to periodic BCs for a number of sites, L , that are multiples of 4 and antiperiodic BCs for even L that are not multiples of 4.

For fixed U , small Δ , and half filling as assumed here, the system is in the MI phase with zero spin gap. Increasing Δ , at the point $\Delta = \Delta_s$, a spin gap ΔE_S opens, signaling the transition to the SDI phase. The transition is of the Kosterlitz-Thouless type [4]. Although the spin gap is exponentially small near the transition, the MCEL allows one to identify it unambiguously and accurately from the crossing of the even singlet with lowest energy and the odd triplet of lowest energy (both states have higher energy than the ground state). Also, at $\Delta = \Delta_s$, the spin Berry phase γ_s [5,31] jumps from π to $0 \pmod{2\pi}$. Further increasing Δ , rather soon, at the point $\Delta = \Delta_c$, a charge transition from the SDI to the BI phase takes place in which the charge reorders. At this point, there is a crossing of the two singlets of lowest energy with opposite parity under inversion. In the BI phase, the ground state is the singlet even under inversion, while it is the odd singlet in the other two phases. All of these states have wave vector 0 for $\Delta \neq 0$. In turn, this crossing leads to a jump in the charge Berry phase γ_c from π to $0 \pmod{2\pi}$. As explained above, for $\Delta = \Delta_c$ and using OSBCs, the charge gap ΔE_C defined as the absolute value of the difference in energy between the ground state and the first excited state at half filling (called exciton gap [6] or internal gap [35] in other works) vanishes at the charge transition.

Changes in γ_c are proportional to changes in the polarization. Actually, calculations of the charge Berry phase form the basis of the modern theory of polarization [44–52]. A jump in π in γ_c is consistent with a displacement of an electronic charge per unit cell in half a unit cell (to the next site), on average. This is the change of polarization that corresponds to the change in site occupancies from 1111... to 2020... The IHM in a ring has inversion symmetry with center at any site [43] and, as a consequence, γ_c and γ_s can only be 0 or $\pi \pmod{2\pi}$. In other words, they are Z_2 topological numbers protected by inversion symmetry [44].

If a modulation of the hopping δ is introduced, the inversion symmetry is lost and γ_c can change continuously. This permits one to transfer one charge to the next unit cell in a Thouless pump cycle in the (Δ, δ) plane (see Fig. 1). This can be understood as follows. Starting at a point $(\Delta_1, 0)$ with $\Delta_1 > \Delta_c$, $\gamma_c = 0$. Then, introducing a finite δ , with the appropriate sign, γ_c increases continuously with increasing $|\delta|$. Decreasing Δ to a value $\Delta_2 < \Delta_c$ and returning δ to zero, the point $(\Delta_2, 0)$ is reached where $\gamma_c = \pi$. Continuing the cycle with the opposite sign of δ , γ_c continues to increase and reaches the value $\gamma_c = 2\pi$ at the end of the cycle at $(\Delta_1, 0)$. This corresponds to the displacement of one unit charge by one unit cell according to the modern theory of polarization. The values of the Berry phases in the cycle and time-dependent calculations of the charge transferred have been presented in Ref. [35]. Moreover, this pumping procedure has been recently realized experimentally [36], allowing one to study the effects of interactions in the field of quantized

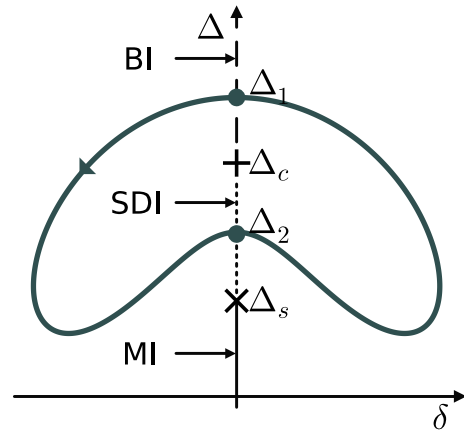


FIG. 1. Schematic representation of the pump trajectory. Dashed, dotted, and solid lines indicate the BI, SDI, and MI phases of the IHM (at $\delta = 0$), respectively.

topological charge pumping in driven systems, which has been of great interest in recent years [37,53].

A problem with the pumping cycle mentioned above is that it usually crosses the MI segment between the points $(\Delta_s, 0)$ and $(-\Delta_s, 0)$ at which the spin gap vanishes. Since unavoidably this segment is traversed at a finite speed, spin excitations are created, leading to the loss of adiabatic quantized pumping [35,36] (we note that introducing δ in the MI phase, a spin gap ΔE_S opens proportional to $|\delta|^{2/3}$ for small δ [35]). To avoid this problem, one might choose the crossing point Δ_2 inside the SDI phase, that is, $\Delta_s < \Delta_2 < \Delta_c$ (as shown in Fig. 1), and then the system is fully gapped in the whole trajectory. However, at $\Delta = \Delta_2$, both gaps ΔE_C and ΔE_S are small and their magnitude is not known. Previous calculations of ΔE_S were affected by strong finite-size effects in the SDI region and were limited to very large values of U [6]. On the other hand, it has been recently shown that the SDI phase is enlarged at small values of U if density-dependent hopping is introduced [32]. A density-dependent hopping can be experimentally engineered by near-resonant Floquet modulation [16–20].

The particular pumping cycle represented in Fig. 1 is motivated by the following reasoning. In the segment $\delta = 0$, $\Delta_s < \Delta < \Delta_c$, both the charge and the spin gaps are finite, but they are small. Introducing δ in the MI phase, a spin gap proportional to $|\delta|^{2/3}$ for small δ [35] rapidly opens and then one can reduce the value of Δ increasing the charge gap, without significantly reducing the spin gap. The competition between both gaps in the above-mentioned segment will become clear in Sec. III.

In this work, we calculate both gaps, ΔE_C and ΔE_S , inside and near the SDI phase, and explore the optimum value of Δ_2 for which the smallest gap is maximum. We use the density-matrix renormalization group (DMRG) method [54–58], as described in Sec. II. We find that to calculate ΔE_S , open BCs are more convenient, while to calculate ΔE_C , a ring with OSBCs leads to the optimum results, improving previous estimates and allowing one to calculate the charge gap within the SDI phase with unprecedented accuracy.

The paper is organized as follows. In Sec. II, we describe the methods used to calculate the gaps. The results are presented in Sec. III. Section IV contains a summary and discussion.

II. METHODS

To perform the energy level calculations, we have used the DMRG method with a code that relies on the ITensors library for JULIA [59]. Conveniently setting S_z sectors, we have calculated ground and excited states with a fixed bond dimension of 900. The truncation error is, in the worst case, of the order of 10^{-6} for periodic BCs (PBCs), and 10^{-10} for open BCs (OBCs).

In general, it is convenient to use OBCs rather than PBCs because the entanglement is lower in the former case, leading to more accurate results in less amount of time. In turn, this fact permits one to reach larger systems. This is particularly important for the spin gap ΔE_S because, even in regions of parameters for which $\Delta E_S = 0$ in the thermodynamic limit, it is finite for finite systems, scaling as $1/L$ for increasing system size L [40]. We have calculated the spin gap by extrapolating the results for different system sizes using a quadratic function in $1/L$. The calculations were done for systems between $L = 40$ and $L = 100$, except in the case of $U = 10$, where we have used sizes up to $L = 64$.

For the charge gap ΔE_C , which is the difference of energies between the first excited state and the ground state in the singlet sector, the situation is different. For OBCs, we find similar difficulties as those found before [6] for calculating the gap in the SDI phase and particularly near the transition to the BI phase, where it should vanish in the thermodynamic limit. The reason is the following. As it is clear using the MCEL method mentioned in Sec. I, the ground state and the first excited state have opposite parity under inversion, being the even state is the one of lowest energy in the BI phase, and both states cross at the BI-SDI transition. For a chain with OBCs and an integer number of unit cells, the inversion symmetry is lost, the crossing becomes an anticrossing, and extrapolation to the thermodynamic limit becomes problematic. Therefore, we change the method using a ring with OSBCs, as described below.

The Lanczos method used in the MCEL has divided the Hilbert space in different symmetry sectors, but the method is limited to 16 sites at half filling [5,30,32]. Our method allows us to use larger system sizes, but we do not have access to the different symmetry sectors. In any case, just plotting the energy of the ground state and first excited state as a function of Δ in a ring, both energy levels and the crossing can be clearly identified. This is illustrated in Fig. 2 for a typical case.

We find that by extrapolating the energies of L that are multiples of 4 for a ring with PBCs (which coincide with OSBCs for the chosen L) between $L = 12$ and $L = 32$ using a quadratic function in $1/L$, an accurate and reliable result for ΔE_C in the thermodynamic limit is obtained. Two examples of the extrapolation are presented in Fig. 3. The second one corresponds to DDH. In both cases, it is clear that as Δ increases, the separation between the extrapolated values of the charge gap also increases. In other words, the slopes of the gap as a function of Δ are different at both sides of

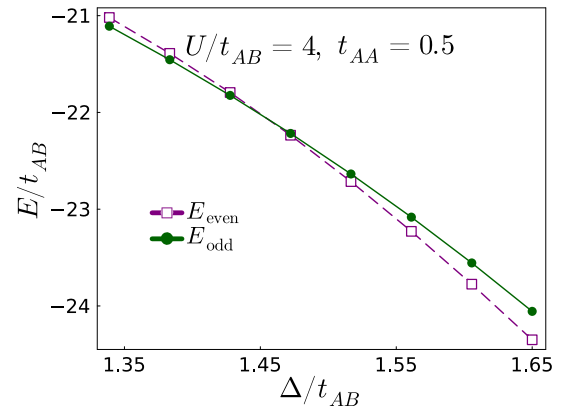


FIG. 2. Ground state and first excited state as a function of Δ for 32 sites and PBCs.

the transition. Taking into account this fact, we find that the difference between the odd and even states can be well fitted by the following function with four parameters:

$$E_{\text{odd}} - E_{\text{even}} = (\Delta - \Delta_c) \left[A + B \tanh \left(\frac{\Delta - \Delta_c}{C} \right) \right]. \quad (2)$$

Examples will be shown in the next section.

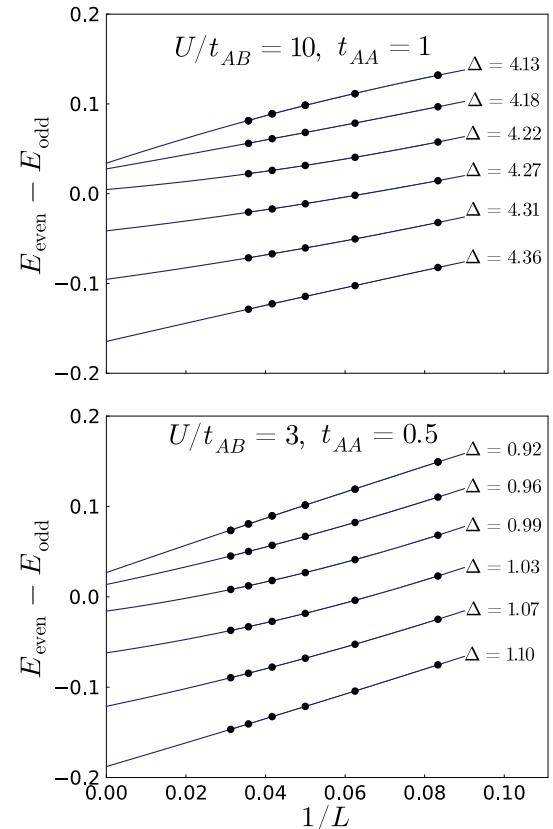


FIG. 3. Difference of energy between the even and odd states of lowest energy as a function of the inverse of the systems size L for all L that are multiples of 4 in the range $12 \leq L \leq 32$ with PBCs for several values of Δ and two sets of other parameters. The transition is calculated to be at $\Delta_c = 4.226$ (0.978) for the top (bottom) figure.

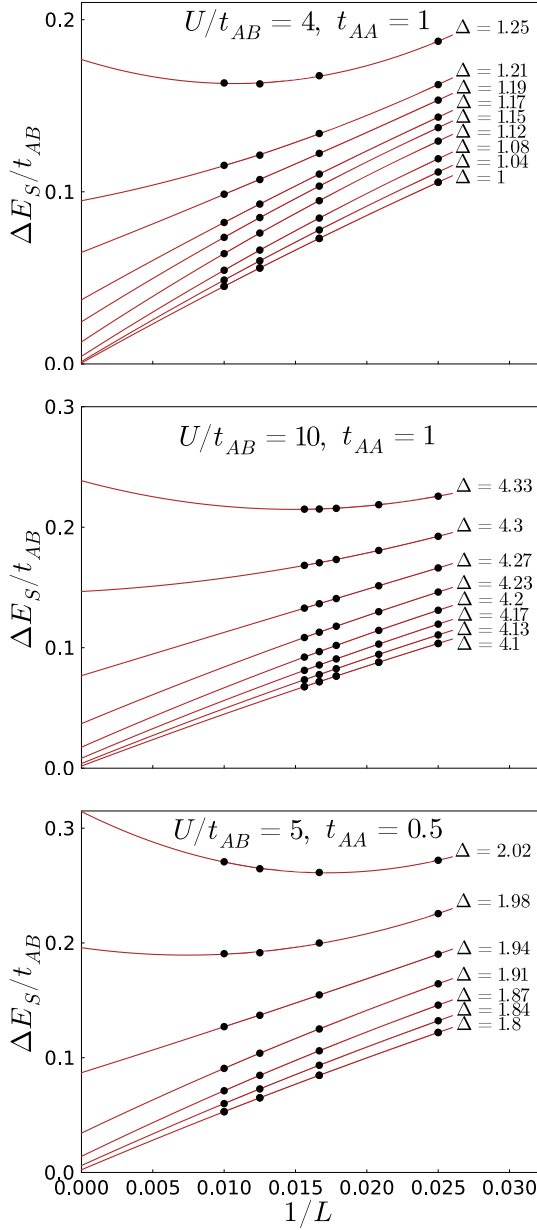


FIG. 4. Spin gap as a function of the inverse of the systems size L with PBCs for parameters indicated inside each figure.

Comparing with previous results using the MCEL in smaller systems [32], we have also found that using OSBCs, the crossing between the first excited state in the sector with total spin projection $S_z = 0$ (corresponding to the even singlet [32]) and the lowest-energy state in the sector with $S_z = 1$ (an odd triplet [32]) corresponds to the crossing at $\Delta = \Delta_s$ that signals the opening of the spin gap ΔE_S , and the SDI-MI transition, as explained in Sec. I.

Therefore, our methods might also be used to improve the accuracy of the phase diagrams calculated with the MCEL, extending the results to larger systems.

In Fig. 4, we show three examples (the last one with DDH) of the extrapolation of the spin gap, calculated as the difference in energy between the lowest states in the sectors with $S_z = 1$ and $S_z = 0$ using OBCs. When the extrapolated gap is

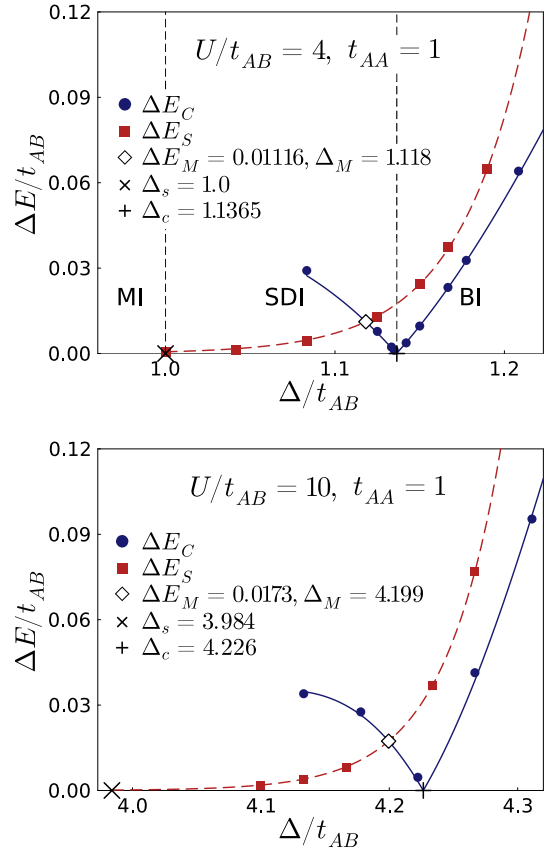


FIG. 5. Charge gap (blue circles) and spin gap (red squares) as a function of Δ for two values of U and $t_{AA} = t_{BB} = t_{AB} = 1$. Blue solid [red dashed] line is a fit using Eq. (2) [Eq. (3)]. Vertical lines in the top figure separate the different phases of the IHM.

very small, the dependence of the spin gap with size behaves like $1/L$, as expected from conformal-field theory in a system without spin gap [40]. For the top figure, the gap is expected to vanish at $\Delta_s = 1$ using the above-described MCEL up to 28 sites. The extrapolated value of the spin gap turns out to be of the order of 10^{-4} , which provides an estimation of the error in the spin gap.

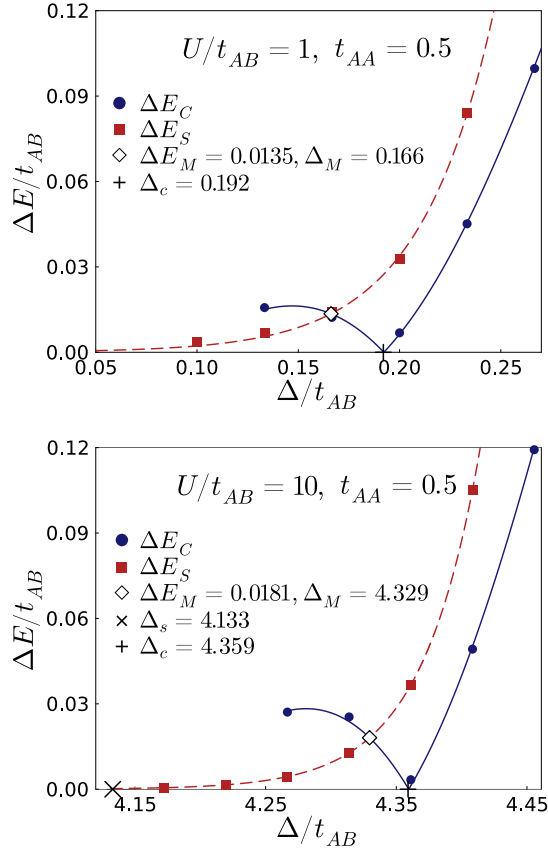
We have found empirically that sufficiently far from Δ_s and in the SDI phase, or in the BI phase near the SDI-BI transition at $\Delta = \Delta_c$, the dependence on Δ of the spin gap is well described by the expression

$$\Delta E_S = A_s \exp[B_s(\Delta - C_s)]. \quad (3)$$

III. RESULTS

In this section, we describe our results for the charge and spin gaps in the IHM with DDH [Eq. (1) with $\delta = 0$ and $t_{BB} = t_{AA}$]. We also take $t_{AB} = 1$ as the unit of energy.

In Fig. 5, we show the gaps for the model without DDH and two values of U . The maximum difference between any excited state and the ground state in the SDI phase is denoted by ΔE_M . This value is obtained at the crossing between both studied gaps. The value of Δ at this crossing is denoted as Δ_M . We also denote, by a cross on the axis of the abscissa in

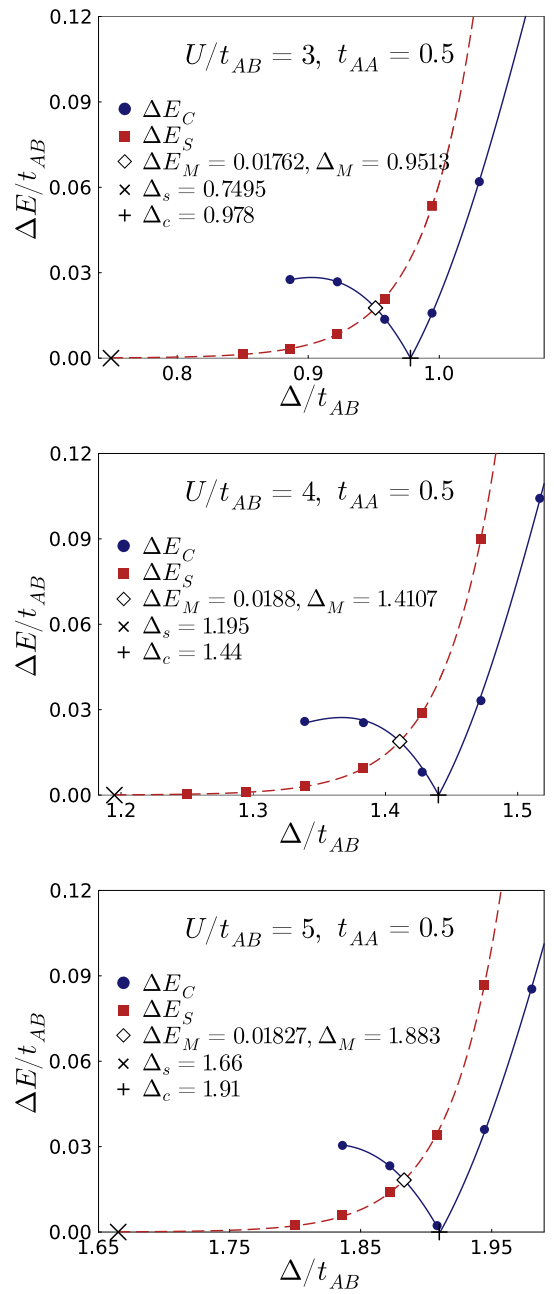
FIG. 6. Same as Fig. 5 for $t_{AA} = t_{BB} = 0.5$ and $t_{AB} = 1$.

the figures, the point at which the spin gap closes according to the MCEL, as described in Sec. II.

From the figures, one can see that the spread of the SDI phase, $\Delta_c - \Delta_s$ (near 0.14 for $U = 4$ and 0.24 for $U = 10$), and also ΔE_M (about 0.011 for $U = 4$ and 0.017 for $U = 10$) is larger for larger values of U than for moderate ones. The former fact is in agreement with calculations of the phase diagram using up to 16 sites [5], although $\Delta_c - \Delta_s$ is a little bit smaller in our case. Our values should be more accurate since we have calculated Δ_c and Δ_s using up to 32 and 28 sites, respectively.

In Fig. 6, we analyze the effect of DDH, decreasing $t_{AA} = t_{BB}$ to half the value of $t_{AB} = 1$, for two extreme values of U , leaving the intermediate values of U for Fig. 7. For $U = 10$, the maximum value of the gap ΔE_M (near 0.0181) *increases* slightly with respect to the case $t_{AA} = t_{BB} = 1$ (0.0173). This effect is rather surprising because one naively expects that by reducing the average value of the hopping, both ΔE_M and the amplitude of the SDI phase should decrease. Therefore, the effect of introducing DDH overcomes the effect of reducing the average hopping regarding ΔE_M . Instead, the amplitude of the SDI phase, $\Delta_c - \Delta_s$, decreases slightly (0.226 compared to 0.242).

As discussed earlier [32], for small values of U , the amplitude of the SDI phase increases markedly since it continues to exist even for $\Delta = 0$. However, the magnitude of the maximum gap ΔE_M is reduced by 25% (to 0.0135) when U is reduced from 10 to 1.

FIG. 7. Same as Fig. 6 for intermediate values of U .

In order to look for the largest possible value of ΔE_M in the presence of DDH, we have calculated the gaps for intermediate values of U . The result is shown in Fig. 7. While, qualitatively, the results for $U = 3, 4$, and 5 are similar, differing by less than 7% for these values of U , the maximum gap $\Delta E_M = 0.0188$ is obtained for $U = 4$. Instead, the maximum spread of the SDI phase (0.25) is obtained for $U = 5$, but it is only 2% larger than the corresponding value for $U = 4$.

IV. SUMMARY AND DISCUSSION

We have calculated the charge and spin gaps of the spontaneously dimerized insulating (SDI) phase of the ionic Hubbard model, including electron-hole symmetric

density-dependent hopping. We have developed a method using the DMRG method to calculate the charge gap, which presents advantages with respect to previously used ones, leading to substantially more accurate values. In addition, phase diagrams constructed by the method of crossing of energy levels might be calculated more accurately than using only Lanczos methods, if they are combined with the DMRG method (the former can be used to identify the symmetry sectors).

The results might be useful to present experiments with cold atoms in which quantized Thouless pumping of one charge is observed, when a pump cycle in the two-dimensional space (Δ, δ) enclosing the point $(\Delta_c, 0)$ is performed in a realization of the interacting Rice-Mele model [Eq. (1)], where Δ_c is the value of Δ at the transition between the SDI and the band insulating (BI) phase. A fully adiabatic pump is possible if the Mott insulating (MI) phase is avoided. This phase lies at the segment between the points $(\Delta_s, 0)$ and $(-\Delta_s, 0)$, where $\pm\Delta_s$ are the points of the MI-SDI phase transitions. For this purpose, the SDI phase should be traversed.

Fixing $t_{AB} = 1$, we find that the maximum gap inside the SDI phase is about 0.019. This is a rather small value, which by simple estimates seems to require a velocity about 10 times smaller than that used in available experiments [36] to guarantee adiabatic pumping in crossing the point $(\Delta_M, 0)$. However introducing δ , the gap increases quickly (as $|\delta|^{2/3}$ in the MI phase). A time-dependent calculation, possibly decreasing the velocity near $(\Delta_M, 0)$, would be useful to check this procedure.

The effect of density-dependent hopping, reducing $t_{AA} = t_{BB}$ and keeping $t_{AB} = 1$, is moderate in increasing the gap, although it is important if the average hopping is kept at the same value. Its main effect is that for small U , the extension of the fully gapped SDI phase is strongly increased.

ACKNOWLEDGMENTS

A.A.A. (K.H.) acknowledges financial support provided by PICT Grant No. 2020A 03661 and PICT Grant No. 2018-01546 of the Agencia I+D+i, Argentina. K.H. acknowledges support from ICTP through the Associates Programs.

-
- [1] N. Nagaosa and J.-i. Takimoto, Theory of neutral-ionic transition in organic crystals. I. Monte Carlo simulation of modified Hubbard model, *J. Phys. Soc. Jpn.* **55**, 2735 (1986).
- [2] J. B. Torrance, A. Girlando, J. J. Mayerle, J. I. Crowley, V. Y. Lee, P. Batail, and S. J. LaPlaca, Anomalous nature of neutral-to-ionic phase transition in Tetrathiafulvalene-Chloranil, *Phys. Rev. Lett.* **47**, 1747 (1981).
- [3] T. Egami, S. Ishihara, and M. Tachiki, Lattice effect of strong electron correlation: Implication for ferroelectricity and superconductivity, *Science* **261**, 1307 (1993).
- [4] M. Fabrizio, A. O. Gogolin, and A. A. Nersisyan, From band insulator to mott insulator in one dimension, *Phys. Rev. Lett.* **83**, 2014 (1999).
- [5] M. E. Torio, A. A. Aligia, and H. A. Ceccatto, Phase diagram of the Hubbard chain with two atoms per cell, *Phys. Rev. B* **64**, 121105(R) (2001).
- [6] S. R. Manmana, V. Meden, R. M. Noack, and K. Schönhammer, Quantum critical behavior of the one-dimensional ionic Hubbard model, *Phys. Rev. B* **70**, 155115 (2004).
- [7] A. A. Aligia, Charge dynamics in the Mott insulating phase of the ionic Hubbard model, *Phys. Rev. B* **69**, 041101(R) (2004).
- [8] C. D. Batista and A. A. Aligia, Exact bond ordered ground state for the transition between the band and the mott insulator, *Phys. Rev. Lett.* **92**, 246405 (2004).
- [9] A. A. Aligia and C. D. Batista, Dimerized phase of ionic Hubbard models, *Phys. Rev. B* **71**, 125110 (2005).
- [10] L. Tincani, R. M. Noack, and D. Baeriswyl, Critical properties of the band-insulator-to-Mott-insulator transition in the strong-coupling limit of the ionic Hubbard model, *Phys. Rev. B* **79**, 165109 (2009).
- [11] A. Hosseinzadeh and S. A. Jafari, Quantum integrability of 1d ionic hubbard model, *Ann. Phys.* **532**, 1900601 (2020).
- [12] A. Hosseinzadeh and S. A. Jafari, Generalization of Lieb-Wu wave function inspired by one-dimensional ionic Hubbard model, *Ann. Phys.* **414**, 168075 (2020).
- [13] M. E. Torio, A. A. Aligia, G. I. Japaridze, and B. Normand, Quantum phase diagram of the generalized ionic Hubbard model for AB_n chains, *Phys. Rev. B* **73**, 115109 (2006).
- [14] L. Stenzel, A. L. C. Hayward, C. Hubig, U. Schollwöck, and F. Heidrich-Meisner, Quantum phases and topological properties of interacting fermions in one-dimensional superlattices, *Phys. Rev. A* **99**, 053614 (2019).
- [15] M. J. Rice and E. J. Mele, Elementary excitations of a linearly conjugated diatomic polymer, *Phys. Rev. Lett.* **49**, 1455 (1982).
- [16] R. Ma, M. E. Tai, P. M. Preiss, W. S. Bakr, J. Simon, and M. Greiner, Photon-assisted tunneling in a biased strongly correlated bose gas, *Phys. Rev. Lett.* **107**, 095301 (2011).
- [17] F. Meinert, M. J. Mark, K. Lauber, A. J. Daley, and H.-C. Nägerl, Floquet engineering of correlated tunneling in the bose-Hubbard model with ultracold atoms, *Phys. Rev. Lett.* **116**, 205301 (2016).
- [18] F. Görg, M. Messer, K. Sandholzer, G. Jotzu, R. Desbuquois, and T. Esslinger, Enhancement and sign change of magnetic correlations in a driven quantum many-body system, *Nature (London)* **553**, 481 (2018).
- [19] M. Messer, K. Sandholzer, F. Görg, J. Minguzzi, R. Desbuquois, and T. Esslinger, Floquet dynamics in driven Fermi-Hubbard systems, *Phys. Rev. Lett.* **121**, 233603 (2018).
- [20] F. Görg, K. Sandholzer, J. Minguzzi, R. Desbuquois, M. Messer, and T. Esslinger, Realization of density-dependent Peierls phases to engineer quantized gauge fields coupled to ultracold matter, *Nat. Phys.* **15**, 1161 (2019).
- [21] H. B. Schüttler and A. J. Fedro, Copper-oxygen charge excitations and the effective-single-band theory of cuprate superconductors, *Phys. Rev. B* **45**, 7588 (1992).
- [22] M. E. Simon and A. A. Aligia, Brinkman-Rice transition in layered perovskites, *Phys. Rev. B* **48**, 7471 (1993).

- [23] J. E. Hirsch and F. Marsiglio, Hole superconductivity: Review and some new results, *Physica C: Supercond. Appl.* **162-164**, 591 (1989).
- [24] L. Arrachea and A. A. Aligia, Pairing correlations in a generalized Hubbard model for the cuprates, *Phys. Rev. B* **61**, 9686 (2000).
- [25] A. A. Aligia, A. Anfossi, L. Arrachea, C. Degli Esposti Boschi, A. O. Dobry, C. Gazza, A. Montorsi, F. Ortolani, and M. E. Torio, Incommensurability and unconventional superconductor to insulator transition in the Hubbard model with bond-charge interaction, *Phys. Rev. Lett.* **99**, 206401 (2007).
- [26] A. O. Dobry and A. A. Aligia, Quantum phase diagram of the half filled Hubbard model with bond-charge interaction, *Nucl. Phys. B* **843**, 767 (2011).
- [27] A. Montorsi, U. Bhattacharya, D. González-Cuadra, M. Lewenstein, G. Palumbo, and L. Barbiero, Interacting second-order topological insulators in one-dimensional fermions with correlated hopping, *Phys. Rev. B* **106**, L241115 (2022).
- [28] W. Chen, J. Zhang, and H. Ding, Ground-state instabilities in a Hubbard-type chain with particular correlated hopping at non-half-filling, *Results Phys.* **49**, 106472 (2023).
- [29] S. Jiang, D. J. Scalapino, and S. R. White, A single-band model with enhanced pairing from DMRG-based downfolding of the three-band Hubbard model, *Phys. Rev. B* **108**, L161111 (2023).
- [30] M. Nakamura, Tricritical behavior in the extended Hubbard chains, *Phys. Rev. B* **61**, 16377 (2000).
- [31] A. A. Aligia, K. Hallberg, C. D. Batista, and G. Ortiz, Phase diagrams from topological transitions: The Hubbard chain with correlated hopping, *Phys. Rev. B* **61**, 7883 (2000).
- [32] P. Roura-Bas and A. A. Aligia, Phase diagram of the ionic Hubbard model with density-dependent hopping, *Phys. Rev. B* **108**, 115132 (2023).
- [33] G. I. Japaridze and A. P. Kampf, Weak-coupling phase diagram of the extended Hubbard model with correlated-hopping interaction, *Phys. Rev. B* **59**, 12822 (1999).
- [34] A. A. Aligia and L. Arrachea, Triplet superconductivity in quasi-one-dimensional systems, *Phys. Rev. B* **60**, 15332 (1999).
- [35] E. Bertok, F. Heidrich-Meisner, and A. A. Aligia, Splitting of topological charge pumping in an interacting two-component fermionic Rice-Mele Hubbard model, *Phys. Rev. B* **106**, 045141 (2022).
- [36] K. Viebahn, A.-S. Walter, E. Bertok, Z. Zhu, M. Gächter, A. A. Aligia, F. Heidrich-Meisner, and T. Esslinger, Interaction-induced charge pumping in a topological many-body system, [arXiv:2308.03756](https://arxiv.org/abs/2308.03756).
- [37] A.-S. Walter, Z. Zhu, M. Gächter, J. Minguzzi, S. Roschinski, K. Sandholzer, K. Viebahn, and T. Esslinger, Quantization and its breakdown in a Hubbard-Thouless pump, *Nat. Phys.* **19**, 1471 (2023).
- [38] M. Nakagawa, T. Yoshida, R. Peters, and N. Kawakami, Breakdown of topological Thouless pumping in the strongly interacting regime, *Phys. Rev. B* **98**, 115147 (2018).
- [39] R. D. Somma and A. A. Aligia, Phase diagram of the XXZ chain with next-nearest-neighbor interactions, *Phys. Rev. B* **64**, 024410 (2001).
- [40] K. Nomura and K. Okamoto, Critical properties of $S = 1/2$ antiferromagnetic XXZ chain with next-nearest-neighbour interactions, *J. Phys. A: Math. Gen.* **27**, 5773 (1994).
- [41] M. Nakamura, K. Nomura, and A. Kitazawa, Renormalization group analysis of the spin-gap phase in the one-dimensional $t - J$ model, *Phys. Rev. Lett.* **79**, 3214 (1997).
- [42] M. Nakamura, Mechanism of CDW-SDW transition in one dimension, *J. Phys. Soc. Jpn.* **68**, 3123 (1999).
- [43] The inversion symmetry in a ring of L sites with center at site i is defined as the operation which interchanges the sites $i - j$ and $i + j \bmod(L)$ for all j .
- [44] A. A. Aligia, Topological invariants based on generalized position operators and application to the interacting Rice-Mele model, *Phys. Rev. B* **107**, 075153 (2023).
- [45] R. Resta, Macroscopic polarization in crystalline dielectrics: The geometric phase approach, *Rev. Mod. Phys.* **66**, 899 (1994).
- [46] D. Xiao, M.-C. Chang, and Q. Niu, Berry phase effects on electronic properties, *Rev. Mod. Phys.* **82**, 1959 (2010).
- [47] D. Vanderbilt, *Berry Phases in Electronic Structure Theory: Electric Polarization, Orbital Magnetization and Topological Insulators* (Cambridge University Press, Cambridge, 2018).
- [48] B. Bradlyn and M. Iraola, Lecture notes on Berry phases and topology, *SciPost Phys. Lect. Notes* **51** (2022).
- [49] G. Ortiz and R. M. Martin, Macroscopic polarization as a geometric quantum phase: Many-body formulation, *Phys. Rev. B* **49**, 14202 (1994).
- [50] R. Resta and S. Sorella, Many-body effects on polarization and dynamical charges in a partly covalent polar insulator, *Phys. Rev. Lett.* **74**, 4738 (1995).
- [51] G. Ortiz, P. Ordejón, R. M. Martin, and G. Chiappe, Quantum phase transitions involving a change in polarization, *Phys. Rev. B* **54**, 13515 (1996).
- [52] X.-Y. Song, Y.-C. He, A. Vishwanath, and C. Wang, Electric polarization as a nonquantized topological response and boundary Luttinger theorem, *Phys. Rev. Res.* **3**, 023011 (2021).
- [53] R. Citro and M. Aidelsburger, Thouless pumping and topology, *Nat. Rev. Phys.* **5**, 87 (2023).
- [54] S. R. White, Density matrix formulation for quantum renormalization groups, *Phys. Rev. Lett.* **69**, 2863 (1992).
- [55] K. A. Hallberg, New trends in density matrix renormalization, *Adv. Phys.* **55**, 477 (2006).
- [56] U. Schollwöck, The density-matrix renormalization group, *Rev. Mod. Phys.* **77**, 259 (2005).
- [57] U. Schollwöck, The density-matrix renormalization group in the age of matrix product states, *Ann. Phys.* **326**, 96 (2011).
- [58] M. C. Bañuls, Tensor network algorithms: A route map, *Annu. Rev. Condens. Matter Phys.* **14**, 173 (2023).
- [59] M. Fishman, S. R. White, and E. M. Stoudenmire, The ITensor software library for tensor network calculations, *SciPost Phys. Codebases* **4** (2022).